

Magnetic order in the chemically-substituted frustrated antiferromagnet CsCrF₄

Shohei Hayashida,^{1,*} Masato Hagihala,^{1,2} Maxim Avdeev,^{3,4}
Yoko Miura,⁵ Hirotaka Manaka,⁶ and Takatsugu Masuda^{1,7}

¹*Institute for Solid State Physics, The University of Tokyo, Kashiwa, Chiba 277-8581, Japan*

²*Neutron Science Division, Institute of Materials Structure Science,
High Energy Accelerator Research Organization, Tsukuba, Ibaraki 305-0801, Japan*

³*Australian Nuclear Science and Technology Organisation,
New Illawarra Rd, Lucas Heights, NSW 2234, Australia*

⁴*School of Chemistry, The University of Sydney, Sydney, NSW 2006, Australia*

⁵*Suzuka National College of Technology, Suzuka, Mie 510-0294, Japan*

⁶*Graduate School of Science and Engineering, Kagoshima University, Korimoto, Kagoshima 890-0065, Japan*

⁷*Trans-scale Quantum Science Institute, The University of Tokyo, Tokyo 113-0033, Japan*
(Dated: January 6, 2022)

The effect of chemical substitution on the ground state of the geometrically frustrated antiferromagnet CsCrF₄ has been investigated through a neutron powder diffraction experiment. Magnetic Fe-substituted CsCr_{0.94}Fe_{0.06}F₄ and nonmagnetic Al-substituted CsCr_{0.98}Al_{0.02}F₄ samples are measured, and magnetic Bragg peaks are clearly observed in both samples. Magnetic structure analysis revealed a 120° structure having a magnetic propagation vector $\mathbf{k}_{\text{mag}} = (0, 0, 1/2)$ in CsCr_{0.94}Fe_{0.06}F₄. For CsCr_{0.98}Al_{0.02}F₄, a quasi-120° structure having $\mathbf{k}_{\text{mag}} = (1/2, 0, 1/2)$ is formed. It is notable that the identified magnetic structure in CsCr_{0.94}Fe_{0.06}F₄ belongs to a different phase of ground states from those in CsCr_{0.98}Al_{0.02}F₄ and the parent CsCrF₄. These results suggest that the Fe substitution strongly influences the ground state of CsCrF₄.

I. INTRODUCTION

Geometrically frustrated magnets have attracted great interest in condensed matter physics because of their exotic magnetic states induced by macroscopic degeneracy of magnetic states at low temperatures [1, 2]. Since the macroscopic degeneracy in the low-energy region can be lifted even by small perturbations, geometrical frustration highlights small effects such as single-ion anisotropy [3, 4], the Dzyaloshinskii-Moriya interaction [5, 6], magnetic dipole-dipole interaction [7, 8], exchange randomness [9–12], and site dilution [13–15]. These may play key roles in determining ground states in frustrated magnets.

The equilateral triangular spin tube antiferromagnet CsCrF₄ is one of the intriguing species in geometrically frustrated magnets [16, 17]. It crystallizes in a hexagonal structure with the space group $P\bar{6}2m$ as illustrated in Fig. 1. The magnetic properties are due to $S = 3/2$ Cr³⁺ ions. It is unique that equilateral triangles formed by CrF₆ octahedra are stacked along the crystallographic c axis, forming triangular spin tubes. These tubes magnetically couple with one another and form the kagome-triangular lattice in the ab plane [18, 19]. Magnetic susceptibility measurements revealed the Curie-Weiss temperature $\theta_{\text{CW}} = -145$ K and a broad maximum at $T \sim 60$ K indicative of developing short-range antiferromagnetic spin correlations [16, 17]. Due to the geometrical frustration and low dimensionality of the triangular spin tube, no clear evidence of a magnetic phase

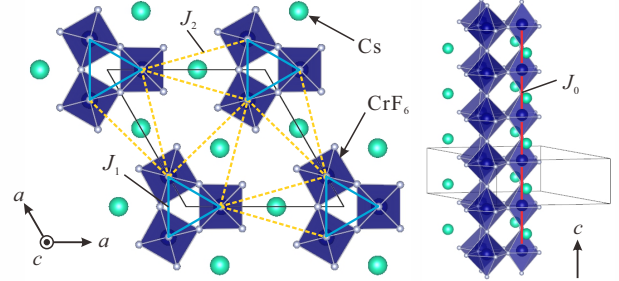


FIG. 1. Schematic view of the crystal structures of CsCrF₄ (hexagonal, space group $P\bar{6}2m$). Red lines indicate the nearest-neighbor interaction along the c axis, J_0 . Blue and yellow lines indicate the nearest- and second-neighbor interactions in the ab plane, J_1 and J_2 .

transition was found in thermodynamic and magnetic measurements [16, 17, 20–22].

In a breakthrough, recent neutron powder diffraction study identified long-range magnetic order of CsCrF₄ below 2.8 K. The magnetic moments form a quasi-120° structure in the ab plane [23]. The 120° structure propagates antiferromagnetically along the a and c axes with a magnetic propagation vector $\mathbf{k}_{\text{mag}} = (1/2, 0, 1/2)$. Discussion of ground states in the kagome-triangular lattice model suggested that the identified 120° structure originates from a ferromagnetic intertube coupling, the Dzyaloshinskii-Moriya interaction, and a strong in-plane single-ion anisotropy. In addition, it was found that the ground state of CsCrF₄ is close to the boundary on the magnetic phase diagram in the kagome-triangular lattice model [23]. This suggests that small perturbations may induce various types of magnetic states in CsCrF₄.

* shoheih@phys.ethz.ch; Present address: Laboratory for Solid State Physics, ETH Zürich, 8093 Zürich, Switzerland

Chemical substitution controls the magnetic state in CsCrF_4 [24, 25]. Thermodynamic and magnetic measurements for chemically substituted $\text{CsCr}_{1-x}\text{Fe}_x\text{F}_4$ and $\text{CsCr}_{1-x}\text{Al}_x\text{F}_4$ showed that the magnetic state is significantly influenced by the chemical composition [25]. An antiferromagnetic transition was clearly observed at 4.5 K for $x = 0.06$ in the magnetic Fe-substituted compound, and the substituted superexchange bond $\text{Cr}^{3+}\text{-F}^-\text{-Fe}^{3+}$ enhanced the in-plane magnetic anisotropy. A glasslike transition appeared at about 5 K for the nonmagnetic Al-substituted compound. In the present paper, we investigate long-range magnetic ordering in chemically substituted frustrated antiferromagnet CsCrF_4 . Magnetic structures of $\text{CsCr}_{0.94}\text{Fe}_{0.06}\text{F}_4$ and $\text{CsCr}_{0.98}\text{Al}_{0.02}\text{F}_4$ are identified by a combination of neutron powder diffraction experiments and magnetic structure analysis. The most notable result is that the Fe-substitution effectively turns the ferromagnetic intertube coupling antiferromagnetic.

II. EXPERIMENTAL DETAILS

Polycrystalline samples of $\text{CsCr}_{0.94}\text{Fe}_{0.06}\text{F}_4$ and $\text{CsCr}_{0.98}\text{Al}_{0.02}\text{F}_4$ were prepared by a solid-state reaction method [16, 25]. The powder samples were loaded in vanadium-made containers, which were in turn installed in a conventional liquid ^4He cryostat. Neutron diffraction measurements were performed at the high resolution powder diffractometer ECHIDNA [26, 27] installed at the OPAL research reactor operated by the Australian Nuclear Science and Technology Organisation (ANSTO). We chose a Ge(331) monochromator to obtain neutrons with a wavelength of 2.4395 Å, and used the open-open-5' configuration. Temperatures were set at 10 K and 1.5 K. The neutron diffraction data were analyzed by the Rietveld method with the FULLPROF software [28]. Candidates for magnetic structures compatible with the lattice symmetry were obtained by the SARAH software [29]. We used the VESTA software [30] for drawing the crystal structures and magnetic structures.

III. RESULTS AND ANALYSIS

Figures 2(a) and 2(b) show neutron powder diffraction profiles at 10 K for $\text{CsCr}_{0.94}\text{Fe}_{0.06}\text{F}_4$ and $\text{CsCr}_{0.98}\text{Al}_{0.02}\text{F}_4$, respectively. These are reasonably fitted by the hexagonal structure with the space group $P\bar{6}2m$. Obtained profile factors are $R_{\text{wp}} = 7.33\%$ and $R_e = 3.70\%$ for $\text{CsCr}_{0.94}\text{Fe}_{0.06}\text{F}_4$, and $R_{\text{wp}} = 9.26\%$ and $R_e = 5.01\%$ for $\text{CsCr}_{0.98}\text{Al}_{0.02}\text{F}_4$. The refined lattice and structural parameters (Table I) are consistent with the previous results measured by x-ray powder diffraction experiments [24, 25]. We conclude that the crystal structures are retained at low temperatures.

Figure 3 shows neutron diffraction profiles at 1.5 and 10 K, which are below and above the transition temper-

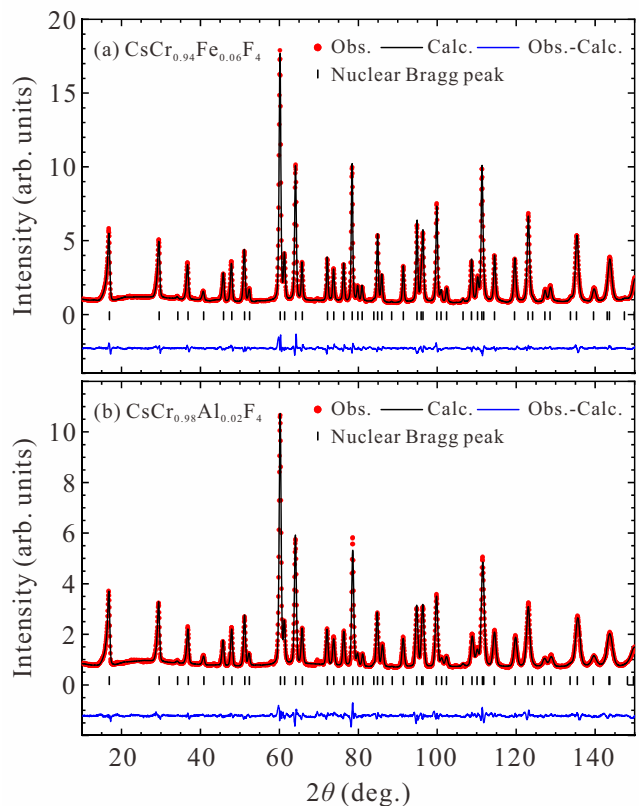


FIG. 2. Neutron powder diffraction profiles for (a) $\text{CsCr}_{0.94}\text{Fe}_{0.06}\text{F}_4$ and (b) $\text{CsCr}_{0.98}\text{Al}_{0.02}\text{F}_4$ measured at 10 K. Red squares and black curves show the experimental data and simulations, respectively. Vertical bars indicate the position of the nuclear Bragg peaks. Solid curves below the bars show the difference between the data and simulations.

TABLE I. Results of the structural refinement in space group $P\bar{6}2m$ of the neutron powder diffraction profiles measured at $T = 10$ K for $\text{CsCr}_{0.94}\text{Fe}_{0.06}\text{F}_4$ and $\text{CsCr}_{0.98}\text{Al}_{0.02}\text{F}_4$.

$\text{CsCr}_{0.94}\text{Fe}_{0.06}\text{F}_4$	
a (Å)	9.56402(7)
c (Å)	3.85832(3)
Cs (3g)	(0.57202(12), 0, 1/2)
Cr and Fe (3f)	(0.22456(23), 0, 0)
F (3f)	(0.83226(14), 0, 0)
F (3g)	(0.22024(15), 0, 1/2)
F (6j)	(0.43914(10), 0.16142(11), 0)
$\text{CsCr}_{0.98}\text{Al}_{0.02}\text{F}_4$	
a (Å)	9.56886(6)
c (Å)	3.85059(3)
Cs (3g)	(0.57203(17), 0, 1/2)
Cr and Al (3f)	(0.22327(36), 0, 0)
F (3f)	(0.83208(19), 0, 0)
F (3g)	(0.22089(21), 0, 1/2)
F (6j)	(0.43801(13), 0.16032(15), 0)

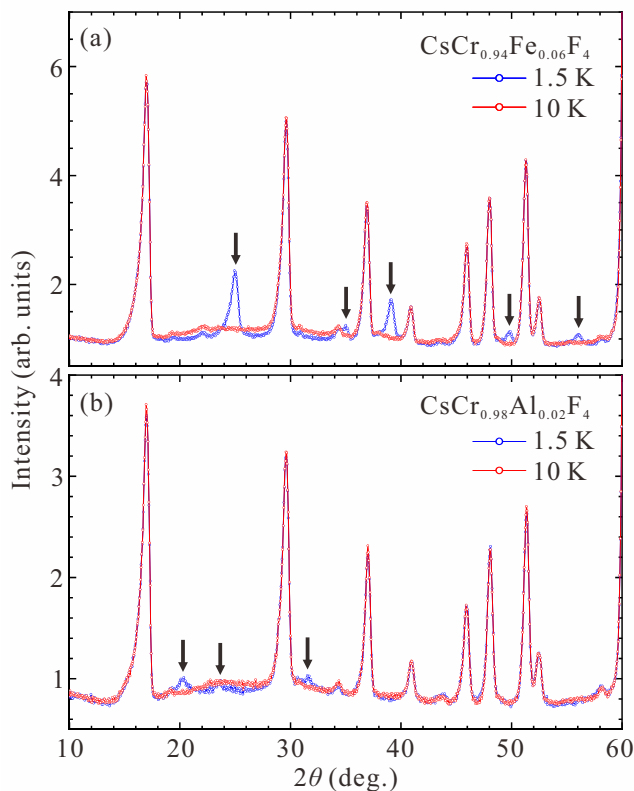


FIG. 3. Neutron powder diffraction profiles for (a) $\text{CsCr}_{0.94}\text{Fe}_{0.06}\text{F}_4$ and (b) $\text{CsCr}_{0.98}\text{Al}_{0.02}\text{F}_4$. Blue and red marks are data measured at 1.5 and 10 K, respectively. Arrows indicate the magnetic Bragg peaks.

ature observed in the magnetic susceptibility data [25]. In both samples, diffuse scattering is observed at 10 K in the range of $20^\circ \leq 2\theta \leq 40^\circ$, and it is suppressed below the transition temperature. This behavior is the same as in CsCrF_4 [23] and indicates that the short-range spin correlations develop at 10 K. For $\text{CsCr}_{0.94}\text{Fe}_{0.06}\text{F}_4$, we clearly see additional peaks at 1.5 K, indicating the long-range magnetic order. Additional peaks are also visible in $\text{CsCr}_{0.98}\text{Al}_{0.02}\text{F}_4$ even though their intensities are weak. This result suggests that the anomaly observed at 5 K in the magnetic susceptibility measurements [25] corresponds to weak long-range magnetic ordering rather than the glasslike transition. Remarkably, the peaks for $\text{CsCr}_{0.94}\text{Fe}_{0.06}\text{F}_4$ are observed at different scattering angles from those in CsCrF_4 , while the peak positions in $\text{CsCr}_{0.98}\text{Al}_{0.02}\text{F}_4$ are the same with CsCrF_4 . Indexing the observed magnetic Bragg peaks results in the magnetic propagation vectors $\mathbf{k}_{\text{mag}} = (0, 0, 1/2)$ for $\text{CsCr}_{0.94}\text{Fe}_{0.06}\text{F}_4$ and $\mathbf{k}_{\text{mag}} = (1/2, 0, 1/2)$ for $\text{CsCr}_{0.98}\text{Al}_{0.02}\text{F}_4$.

To determine magnetic structures that are compatible with the space group symmetry, we performed representation analysis. We assume that a magnetic structure is described by a single irreducible-representation (IR). For $\text{CsCr}_{0.94}\text{Fe}_{0.06}\text{F}_4$, the representation analysis with the space group $P\bar{6}2m$ and the propagation vector

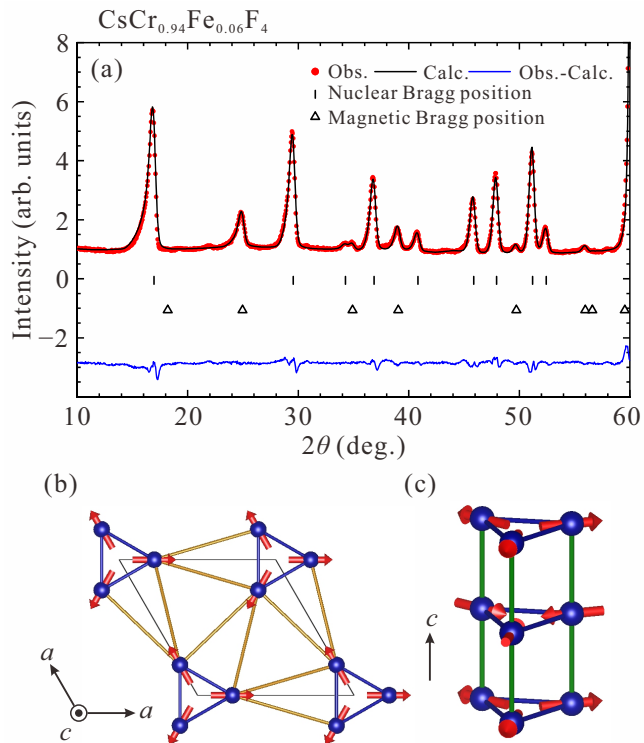


FIG. 4. (a) Neutron diffraction profile for $\text{CsCr}_{0.94}\text{Fe}_{0.06}\text{F}_4$ at 1.5 K. Red squares and black curves show the experimental data and simulations, respectively. Vertical bars and triangles indicate the position of the nuclear and magnetic Bragg peaks. Solid curves below the triangles show the difference between the data and simulations. The magnetic structure of $\text{CsCr}_{0.94}\text{Fe}_{0.06}\text{F}_4$ with Γ_2 (b) in the ab plane and (c) along the c axis.

$\mathbf{k}_{\text{mag}} = (0, 0, 1/2)$ leads to five IRs. The details of the IRs and corresponding basis vectors are listed in Table II. From the Rietveld refinement, a magnetic structure described by Γ_2 gives excellent agreement with the experimental data, as shown in Fig. 4(a). R factors for the whole profile are $R_{\text{wp}} = 8.67\%$ and $R_e = 3.86\%$. The magnetic R factor is $R_{\text{mag}} = 7.40\%$. Note that small peaks at $2\theta = 22^\circ$ and 58° are likely due to nonmagnetic impurities because they are also observed at 10 K. In the identified magnetic structure, the magnetic moments form a 120° structure in the ab plane, and they propagate antiferromagnetically along the c axis, as displayed in Figs. 4(b) and 4(c). The averaged magnitude of the magnetic moment is evaluated to be $1.66(1) \mu_B$. Since an effective magnetic moment for $\text{Cr}_{0.94}^{3+}\text{Fe}_{0.06}^{3+}$ is provided by $3.12 \mu_B (= 0.94 \times 3 \mu_B + 0.06 \times 5 \mu_B)$, the refined moment size is much smaller than the effective one. This is the same result as that in the parent CsCrF_4 [23]. This implies that the magnetic moment strongly fluctuates even at 1.5 K due to the geometrical frustration and low dimensionality.

For $\text{CsCr}_{0.98}\text{Al}_{0.02}\text{F}_4$, the representation analysis with the space group $P\bar{6}2m$ and the propagation vector $\mathbf{k}_{\text{mag}} = (1/2, 0, 1/2)$ leads to splitting of the three equiv-

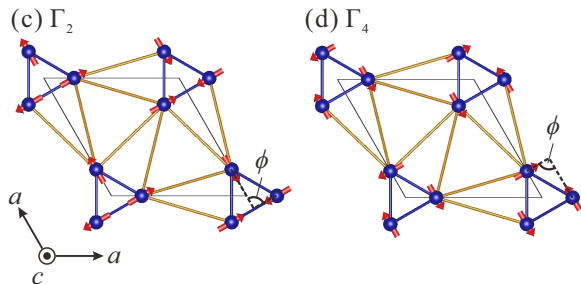
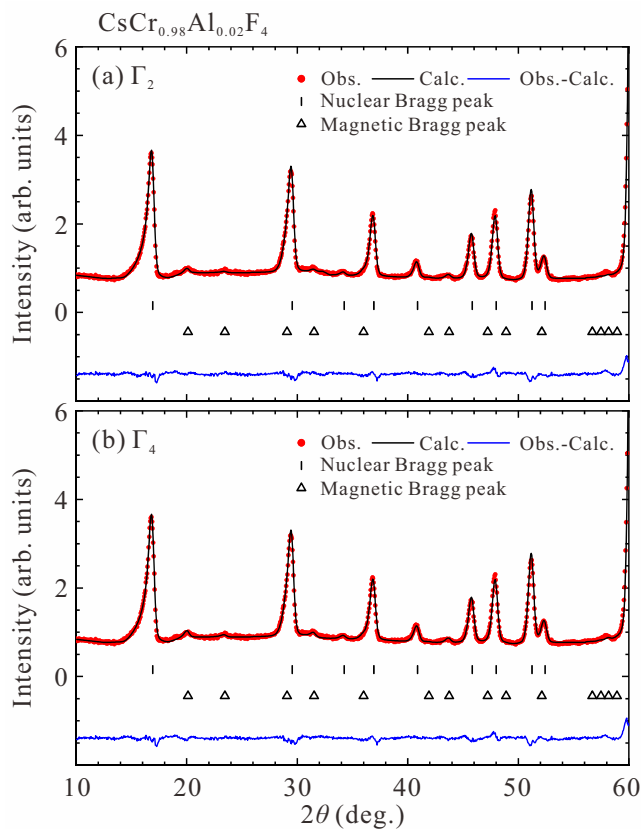


FIG. 5. Refined diffraction profiles for $\text{CsCr}_{0.98}\text{Al}_{0.02}\text{F}_4$ at 1.5 K. The IRs of the magnetic structure for the simulations are (a) Γ_2 and (b) Γ_4 , respectively. Red squares and black curves show the experimental data and simulations, respectively. Vertical bars and triangles indicate the position of the nuclear and magnetic Bragg peaks. Solid curves below the triangles show the difference between the data and simulations. The magnetic structures of $\text{CsCr}_{0.98}\text{Al}_{0.02}\text{F}_4$ with (c) Γ_2 and (d) Γ_4 .

alent Cr sites into the two nonequivalent Cr sites; site-1 (0.2233, 0, 0), (0.7767, 0.7767, 0), and site-2 (0, 0.2233, 0). Four and three IRs are associated with the site-1 and site-2, respectively. The details of the IRs and corresponding basis vectors are listed in Table III. From the Rietveld refinement, magnetic structures in Γ_2 and Γ_4 give satisfactory agreement with the experimental data, as shown in Figs. 5(a) and 5(b). R factors for the whole profile are $R_{\text{wp}} = 9.59\%$ and $R_e = 5.05\%$ for Γ_2 , and $R_{\text{wp}} = 9.65\%$ and $R_e = 5.06\%$ for Γ_4 . Magnetic R fac-

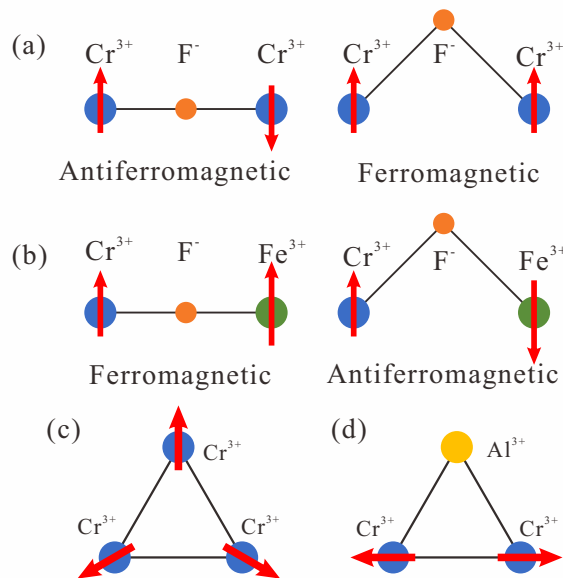


FIG. 6. (a) Superexchange interactions between the Cr^{3+} ions in 180° and 90° bonds via the F^- ion. (b) Superexchange interactions between the Cr^{3+} and Fe^{3+} ions in 180° and 90° bonds via the F^- ion. [(c) and (d)] Spin structures with an antiferromagnetic interaction on an equilateral triangle.

tors are $R_{\text{mag}} = 18.8\%$ for Γ_2 and $R_{\text{mag}} = 15.8\%$ for Γ_4 . Note that it is hard to judge the optimal structure from these results because of the weak intensities of the magnetic Bragg peaks. The identified magnetic structures with $\mathbf{k}_{\text{mag}} = (1/2, 0, 1/2)$ are similar to that in the parent CsCrF_4 , [see Figs. 5(c) and 5(d)]. A quasi- 120° structure is formed in the ab plane, and it propagates antiferromagnetically along the a and c axes. Relative angles ϕ between the moments at the sites 1 and 2, as indicated in Figs. 5(c) and 5(d), are 92.4° for Γ_2 and 90.4° for Γ_4 . These angles deviate more from 120° than 119.5° (Γ_2) and 108° (Γ_4) in CsCrF_4 [23]. Refined magnitude of the magnetic moments is $1.04(7)\mu_B$ for Γ_2 and $1.14(6)\mu_B$ for Γ_4 . As well as that of $\text{Cr}_{0.94}^{3+}\text{Fe}_{0.06}^{3+}$, the refined moment size of $\text{CsCr}_{0.98}\text{Al}_{0.02}\text{F}_4$ is much smaller than the effective moment $2.94\mu_B = (0.98 \times 3\mu_B)$ for $\text{Cr}_{0.98}^{3+}\text{Al}_{0.02}^{3+}$. Thus, the ordered moments are strongly suppressed by the geometrical frustration and low dimensionality in the chemically substituted CsCrF_4 .

IV. DISCUSSION

In the magnetic structure analysis, the 120° structure having $\mathbf{k}_{\text{mag}} = (0, 0, 1/2)$ is found for $\text{CsCr}_{0.94}\text{Fe}_{0.06}\text{F}_4$. In the identified structure, the intertube spin configuration is different from that in the parent CsCrF_4 , but the intratube structure is the same. Let us discuss Fe-substitution effect on exchange interactions. According to the Goodenough-Kanamori rules [31, 32], superexchange interactions between the Cr^{3+} ions via the F^- ion are antiferromagnetic for a 180° bond and ferromagnetic

for a 90° bond as displayed in Fig. 6(a). Once the Cr^{3+} ion is substituted by the Fe^{3+} ion, the superexchange interactions in the 180° and 90° bonds are turned into ferromagnetic and antiferromagnetic ones, respectively [Fig. 6(b)]. Since the bond angles of the nearest-neighbor exchange paths along the c axis, J_0 , and in the ab plane, J_1 , (see Fig. 1) are 178° and 148° in CsCrF_4 [23], their exchange interactions likely turn antiferromagnetic into ferromagnetic by the Fe-substitution. However, the identified magnetic structure in the triangular tube retains the same structure as that in CsCrF_4 . This means that the bond substitution in the intratube coupling has no real effect other than to create a small number of ferromagnetically coupled pairs.

On the contrary, the spin configuration between the spin tubes is totally different from that in CsCrF_4 . In $\text{CsCr}_{0.94}\text{Fe}_{0.06}\text{F}_4$, the magnetic propagation vector in the kagome-triangular plane \mathbf{k}_{2D} is $(0, 0)$. It contrasts with $\mathbf{k}_{2D} = (1/2, 0)$ in CsCrF_4 . This indicates that the substitution drastically changes the ground state even though intertube exchange paths are complicated. In fact, according to the phase diagram of magnetic structures for the kagome-triangular lattice model [19, 23], 120° structures having $\mathbf{k}_{2D} = (0, 0)$ and $(1/2, 0)$ require antiferromagnetic and ferromagnetic intertube couplings, respectively. We note that in the phase diagram the variation of the in-plane anisotropy described in Ref. [25] does not change the intertube spin configuration. Therefore, we conclude that in the magnetic Fe substitution the ground state is modified due to the evolution of the intertube coupling J_2 from ferromagnetic to antiferromagnetic.

The magnetic structure in $\text{CsCr}_{0.98}\text{Al}_{0.02}\text{F}_4$ is not changed drastically, even though the relative angle ϕ between the spins deviates more from 120° than that in the parent CsCrF_4 . On the basis of the classical vector-spin model, spins with the antiferromagnetic interaction form a 120° structure on an equilateral triangle, as displayed in Fig. 6(c). Substituting the Cr^{3+} ion by the Al^{3+} ion creates a spin vacancy in the triangle. This likely induces the remaining two spins to align antiferromagnetically [Fig. 6(d)]. Consequently, the Al substitution breaks a 120° structure locally. However, the spin vacancy only produces a small effect on the ground state of CsCrF_4 , and therefore the quasi- 120° structure is still realized globally in $\text{CsCr}_{0.98}\text{Al}_{0.02}\text{F}_4$.

V. CONCLUSION

In conclusion, we have studied magnetic orders in magnetic Fe- and nonmagnetic Al-substituted CsCrF_4

through a neutron powder diffraction experiment. Magnetic structure analysis reveals that the Fe-substituted sample exhibits a 120° structure having $\mathbf{k}_{\text{mag}} = (0, 0, 1/2)$, and the Al-substituted one has a quasi- 120° structure having $\mathbf{k}_{\text{mag}} = (1/2, 0, 1/2)$. Importantly, the magnetic structure in $\text{CsCr}_{0.94}\text{Fe}_{0.06}\text{F}_4$ differs from that in the parent CsCrF_4 . This result suggests that the ground state in CsCrF_4 is more sensitive to magnetic rather than nonmagnetic substitution on the Cr site. Further studies of magnetic excitation for the Fe-substituted CsCrF_4 would be important to elucidate the spin interactions.

ACKNOWLEDGMENTS

We acknowledge the support of the Australian Centre for Neutron Scattering, Australian Nuclear Science and Technology Organisation, in providing the neutron research facilities used in this work. The neutron diffraction experiments performed using ECHIDNA at ANSTO, Australia were supported by the General User Program for Neutron Scattering Experiments, Institute for Solid State Physics, The University of Tokyo (Proposals No. 18520), at JRR-3, Japan Atomic Energy Agency, Tokai, Japan. S.H. was supported by the Japan Society for the Promotion of Science through the Leading Graduate Schools (MERIT).

TABLE II. Basis vectors for the space group $P\bar{6}2m$ with $\mathbf{k}_{\text{mag}} = (0, 0, 1/2)$. The atoms are defined according to Cr1: $(0.2246, 0, 0)$, Cr2: $(0, 0.2246, 0)$, Cr3: $(0.7754, 0.7754, 0)$.

IRs	Basis Vectors [m_a m_b m_c]		
	Cr1	Cr2	Cr3
Γ_2 Ψ_1 [1 0 0]		[0 1 0]	[-1 -1 0]
Γ_3 Ψ_2 [0 0 1]		[0 0 1]	[0 0 1]
Γ_4 Ψ_3 [1 2 0]		[-2 -1 0]	[1 -1 0]
Γ_5 Ψ_4 [0 0 2]		[0 0 -1]	[0 0 -1]
Ψ_5 [0 0 0]		[0 0 $-\sqrt{3}$]	[0 0 $\sqrt{3}$]
Γ_6 Ψ_6 [2 0 0]		[0 -1 0]	[1 1 0]
Ψ_7 [0 1 0]		[1/2 1/2 0]	[-1/2 0 0]
		$+i[\sqrt{3}/2 \sqrt{3}/2 0]$	$+i[\sqrt{3}/2 0 0]$
Ψ_8 [0 0 0]		[0 $-\sqrt{3}$ 0]	$[-\sqrt{3} -\sqrt{3} 0]$
Ψ_9 [1/2 1/2 0]		[-1/2 0 0]	[0 1 0]
		$+i[-\sqrt{3}/2 -\sqrt{3}/2 0]$	$+i[-\sqrt{3}/2 0 0]$

[1] L. Balents, Nature (London) **464**, 199 (2010).

[2] L. Savary and L. Balents, Rep. Prog. Phys. **80**, 016502 (2017).

TABLE III. Basis vectors for the space group $P\bar{6}2m$ with $\mathbf{k}_{\text{mag}} = (1/2, 0, 1/2)$. The atoms are defined according to Cr1: (0.2233, 0, 0), Cr2: (0, 0.2233, 0), Cr3: (0.7767, 0.7767, 0).

IRs	Basis Vectors [m_a m_b m_c]		
	Cr1	Cr2	
Γ_1 $\Psi_1^{(1)}$	[0 0 1]	[0 0 1]	
Γ_2 $\Psi_2^{(1)}$	[1 0 0]	[1 1 0]	
	$\Psi_3^{(1)}$ [0 1 0]	[0 -1 0]	
Γ_3 $\Psi_4^{(1)}$	[0 0 1]	[0 0 -1]	
Γ_4 $\Psi_5^{(1)}$	[1 0 0]	[-1 -1 0]	
	$\Psi_6^{(1)}$ [0 1 0]	[0 1 0]	
Cr3			
Γ_2 $\Psi_1^{(2)}$	[0 -1 0]		
Γ_3 $\Psi_2^{(2)}$	[0 0 2]		
Γ_4 $\Psi_3^{(2)}$	[2 1 0]		

- [3] R. Moessner, Phys. Rev. B **57**, R5587(R) (1998).
- [4] P.-É. Melchy and M. E. Zhitomirsky, Phys. Rev. B **80**, 064411 (2009).
- [5] M. Elhajal, B. Canals, and C. Lacroix, Phys. Rev. B **66**, 014422 (2002).
- [6] M. Elhajal, B. Canals, R. Sunyer, and C. Lacroix, Phys. Rev. B **71**, 094420 (2005).
- [7] B. C. den Hertog and M. J. P. Gingras, Phys. Rev. Lett. **84**, 3430 (2000).
- [8] M. Maksymenko, V. R. Chandra, and R. Moessner, Phys. Rev. B **91**, 184407 (2015).
- [9] T. E. Saunders and J. T. Chalker, Phys. Rev. Lett. **98**, 157201 (2007).
- [10] A. Andreanov, J. T. Chalker, T. E. Saunders, and D. Sherrington, Phys. Rev. B **81**, 014406 (2010).
- [11] K. Watanabe, H. Kawamura, H. Nakano, and T. Sakai, J. Phys. Soc. Jpn. **83**, 034714 (2014).
- [12] H. Kawamura, K. Watanabe, and T. Shimokawa, J. Phys. Soc. Jpn. **83**, 103704 (2014).
- [13] A. J. Garcia-Adeva and D. L. Huber, Phys. Rev. B **64**, 172403 (2001).
- [14] V. S. Maryasin and M. E. Zhitomirsky, Phys. Rev. Lett. **111**, 247201 (2013).
- [15] A. Andreanov and P. A. McClarty, Phys. Rev. B **91**, 064401 (2015).
- [16] H. Manaka, Y. Hirai, Y. Hachigo, M. Mitsunaga, M. Ito, and N. Terada, J. Phys. Soc. Jpn. **78**, 093701 (2009).
- [17] H. Manaka, T. Etoh, Y. Honda, N. Iwashita, K. Ogata, N. Terada, T. Hisamatsu, M. Ito, Y. Narumi, A. Kondo, K. Kindo, and Y. Miura, J. Phys. Soc. Jpn. **80**, 084714 (2011).
- [18] H. Ishikawa, T. Okubo, Y. Okamoto, and Z. Hiroi, J. Phys. Soc. Jpn. **83**, 043703 (2014).
- [19] K. Seki and K. Okunishi, Phys. Rev. B **91**, 224403 (2015).
- [20] H. Manaka and Y. Miura, J. Phys.: Conf. Ser. **320**, 012043 (2011).
- [21] H. Manaka and Y. Miura, J. Korean Phys. Soc. **62**, 2032 (2013).
- [22] H. Manaka, M. Hagihala, S. Hayashida, M. Soda, T. Masuda, and Y. Miura, Phys. Procedia, **75**, 718 (2015).
- [23] M. Hagihala, S. Hayashida, M. Avdeev, H. Manaka, H. Kikuchi, and T. Masuda, npj Quantum Mater. **4**, 14 (2019).
- [24] Y. Miura and H. Manaka, J. Phys.: Conf. Ser. **320**, 012044 (2011).
- [25] H. Manaka, H. Morita, T. Akasaka, Y. Miura, M. Hagihala, S. Hayashida, M. Soda, and T. Masuda, J. Phys. Soc. Jpn. **88**, 114703 (2019).
- [26] K.-D. Liss, B. Hunter, M. Hagen, T. Noakes, and S. Kennedy, Physica B **385-386**, 1010 (2006).
- [27] M. Avdeev and J. R. Hester, J. Appl. Cryst. **51**, 1597 (2018).
- [28] J. Rodriguez-Carvajal, Physica B **192**, 55 (1993).
- [29] A. Wills, Physica B **276-278**, 680 (2000).
- [30] K. Momma and F. Izumi, J. Appl. Crystallogr. **44**, 1272 (2011).
- [31] J. B. Goodenough, Phys. Rev. **100**, 564 (1955).
- [32] J. Kanamori, J. Phys. Chem. Solids **10**, 87 (1959).